Catena 130 (2015) 69–81

Contents lists available at ScienceDirect

Catena

journal homepage: www.elsevier.com/locate/catena

Lower Rhine historical flood magnitudes of the last 450 years reproduced from grain-size measurements of flood deposits using End Member Modelling

W.H.J. Toonen [a,b,*], T.G. Winkels [a], K.M. Cohen [a,b], M.A. Prins [c], H. Middelkoop [a]

[a] Department of Physical Geography, Utrecht University, Utrecht, The Netherlands
[b] Department of Applied Geology and Geophysics, Deltares BGS, Utrecht, The Netherlands
[c] Department of Earth Sciences, VU University Amsterdam, Amsterdam, The Netherlands

ARTICLE INFO

Article history:
Received 19 October 2013
Received in revised form 1 December 2014
Accepted 3 December 2014
Available online 29 December 2014

Keywords:
Rhine
Palaeoflood
End-member modelling
Flood deposits
Grain-size distribution
Abandoned channel

ABSTRACT

Objective: The objective of this research was to unlock the potential of fluvial archives to create flood chronologies, based on grain-size characteristics of flood deposits located in two recently formed fluvio-lacustrine sequences.
Methods: Grain-size data was compared with contemporaneous discharge measurements (for the Lower Rhine, The Netherlands). Regression relations between coarse-tail grain-size parameters and measured discharge were established for the last ~240 years, and applied to the older parts of both cores – resulting in peak discharge estimates back to AD ~1550.
Results: Grain-size descriptive parameters such as the 95th percentile and end-member modelling outcomes correlate well with discharge and turn out to be sensitive proxies for inferring flood magnitudes. Locally, geomorphological changes influence the relation between peak discharge magnitudes and flood bed coarseness, but these can be assessed, using continuous flood layer and background sedimentation measurements to standardize grain-size descriptive parameters.
Conclusion/implications: Flood records distilled from sedimentary archives hold great potential for extending existing records of observed discharge and aid establishment of design discharge for flood protection measures and assessment of non-stationarity of the flooding regime due to climatic and anthropogenic forcing.

1. Introduction

Estimates of recurrence times and magnitudes of extreme floods are generally based on the extrapolation of measured discharge data. As these datasets often have a limited length (rarely longer than a century), estimated discharges of extreme floods come with a considerable uncertainty (Klemeš, 2000). To extend discharge data series, recent studies explored resampling of meteorological observations to simulate flood events using coupled rainfall-discharge models (Chbab et al., 2006; te Linde et al., 2010), or considered alternative monitoring stations and water level measurements to reconstruct discharges back to the end of the 18th century (Toonen, 2013a). For a limited number of large floods that occurred before routine measurements started, discharge reconstructions are available that made use of historical and geological palaeoflood stage indicators (Herget and Meurs, 2010; Toonen et al., 2013). These studies provide useful specific information on single events, but palaeoflood inventories are generally discontinuous and fragmentary, which troubles accurate assessment of flooding regime variability, especially over longer periods and in the domain of rarely occurring large events.

As river discharge and flow velocities increase during a flood, increasing amounts of coarse grains are entrained in the suspended load transported in the channel, where it moves as bed-load during normal flow. Once entrained in suspension (part of the channel graded suspended load; Passega, 1977), it exchanges during peak discharge with overbank suspended transport and is conveyed over the inundated floodplain. There, the sediment is deposited at various locations, importantly in local lakes and depressions that act as efficient sediment traps, where coarse grains can settle from suspension relatively quickly. At such sites deposition occurs with every flood when discharge exceeds bankfull levels and floodplains are inundated.

This paper evaluates the suitability of several grain-size descriptors for reconstructing historical flood magnitudes, based on two separate research locations to demonstrate reproducibility. Multiple grain-size descriptive parameters were inferred from grain-size distributions of flood deposits; the median, mean, the mean of the sand (>63 μm) fraction (MS), 95th percentile (P95), and various End Member (EM) distributions (Prins et al., 2000). Although previous studies only used the mean and median in flood magnitude analysis (Beierle et al.,

* Corresponding author at: Heidelberglaan 2, 3584 CS Utrecht.
E-mail address: w.h.j.toonen@gmail.com (W.H.J. Toonen).

http://dx.doi.org/10.1016/j.catena.2014.12.004
0341-8162/

2002; Benedetti, 2003; Arnaud, 2005; Czymzik et al., 2013) or variations in organic content (Nesje et al., 2001; Minderhoud et al., 2013), which provided merely qualitative estimates of flood magnitudes, this paper aims to unlock the potential of P95 and the use of End Member Modelling (EMM; Weltje, 1997; Weltje and Prins, 2007) to describe the coarsest tail of grain-size distributions and to relate this information to peak discharge magnitude. Several studies have shown that variations in sedimentary characteristics, such as geochemical composition and the grain-size distribution of deposits correlate with flood magnitude (e.g., Parris et al., 2010; Berner et al., 2012), but these properties have not been used to reconstruct past flood discharges from flood sediments over longer periods back in time. Reconstructions of historical flood discharges, of which actual discharges are largely unknown as generally only the extent of damage was recorded, can provide an additional source of data in flood frequency analysis, which allows for a better representation of extremes, and can serve as input for studies aimed at assessing non-stationarity of flooding regimes induced by climate change and human impact (Knox, 1993; Toonen, 2013a,b).

In the apex region of the Rhine Delta (Fig. 1) sedimentary sequences were retrieved from two lakes in the floodplain, which acted as sinks for flood deposits. The lake fills contain a flood record that spans the last centuries. The top part of the deposits accumulated during the period of modern discharge measurements in the same region, which made it possible to correlate sedimentary characteristics of flood deposits with discharge. The paper makes use of an extended observational discharge series for the Lobith gauging station back to AD 1772 (Toonen, 2013a), and comparison with detailed historical records. Regression analysis between the various age-depth modelled grain-size parameters of flood beds and measured discharges is used to demonstrate the improvement in flood magnitude prediction resulting from standardized coarse-tail descriptive parameters. The obtained relations are applied for flood magnitude reconstructions beyond the period of overlapping records; i.e., before AD 1772. The resulting palaeoflood chronologies inferred for the individual sites are compared and used to present a Lower Rhine palaeoflood chronology back to AD ~1550. Furthermore, it is discussed how specific environmental settings may complicate the extraction of suitable flood records and affect the performance of the unlocked sedimentary records as a proxy for flood magnitudes.

2. Research area

In the floodplains of the Rhine Delta apex area (Fig. 1), two types of sediment trapping lake environments are common; abandoned channels and dike breach scour holes (in this paper referred to as 'scour holes'). Since AD 1350 rivers have been embanked in the Netherlands (Hesselink, 2002). The embankments prevented sediment conveyance to distal parts of the former floodplain and oxbow lakes in those parts, but accelerated deposition close to the river. Starting in the 19th century, additional measures to regulate discharge to reduce flooding and to improve navigation were carried out, and many meanders were artificially cut off. Abandoned channels, either naturally or artificially cut off, have filled gradually with deposits during successive floods.

Related to embankment, a second type of sink for sediments in the floodplain emerged, as deep scour holes were formed when a dike was breached during a flood (Fig. 1). Scour holes positioned at the river-side of the repaired dike form deep lakes in the floodplain and have been filling gradually with flood deposits. Most scours have penetrated Holocene deposits and reached the underlying, easily-erodible Pleistocene sandy braided river deposits, resulting in occasional scour hole depths exceeding 10 m (e.g., Hesselink et al., 2003; Cremer et al., 2010). Because of the abundant sediment supply in the active floodplain, most scour holes tend to fill completely in several centuries (Middelkoop, 1997). This ensures a high resolution of registered floods.

Two research locations were selected in the vicinity of Lobith (Fig. 1), where discharge data and additional discharge reconstructions are available since AD 1772 (Toonen, 2013a). A scour hole named Zwarte Gat (ZG), formed during the flood of AD 1644 (Buisman, 2000), is located ~25 km downstream of Lobith. From ~15 km upstream of Lobith, in the Lower Rhine Valley, the Bienener Altrhein (BAR) was selected; this is an infilled oxbow lake, which was according to historical descriptions and maps (sGrooten, 1573) abandoned around AD 1550 (Braun and Thiermann, 1981). Site choice was based on proximity to the gauging station of Lobith, and period of registration commencing as early as possible, albeit that part of the sedimentary sequence must be overlapping with discharge measurements. Both sites are located in parts of the floodplain that today inundate when discharge of the Rhine at Lobith exceeds ~6500 $m^3 s^{-1}$.

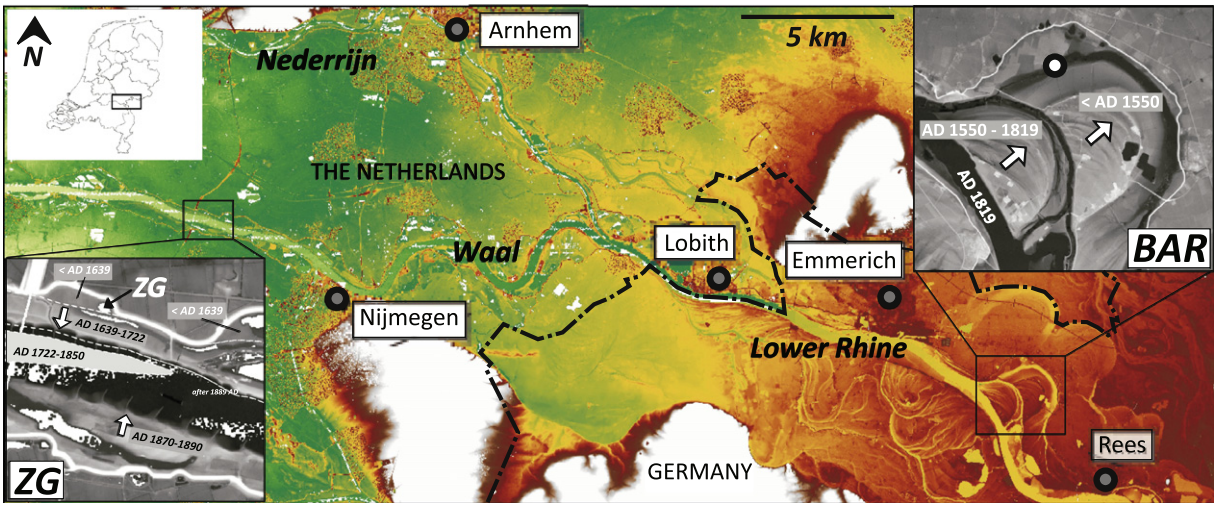

Fig. 1. Floodplain elevation map of the apex region of the Rhine Delta (the Netherlands and Germany; Rijkswaterstaat-AGI, 2005; Cohen et al., 2009) — white and red colours respectively indicate high elevations of the Saalian ice-pushed ridges (20–80 m + msl) and the Lower Rhine Valley (10–20 m + msl), green colours mark the low-lying Rhine Delta (5–10 m + msl). Detail insets show core location surroundings (light = high, dark = low) with the historical development of local morphology (based on historical maps; references in the main text); white arrows and ages indicate the direction and period of fluvial migration.

3. Methods and materials

Cores were retrieved with a modified Livingston piston corer. At site ZG, a first coring campaign in 1991 was ceased after ~9.8 m due to borehole collapse (Middelkoop, 1997). The very base of the fill thus remained unsampled, but is probably not much deeper as historical records mention a 30 ft (~10 m) deep lake directly after formation (Buisman, 2000). The further shallowed pond was revisited in 2011 to collect deposits of the last decades. Geochemical markers (pollutants) in the upper metres allowed correlating corresponding sedimentary layers between both cores. At site BAR, reconnaissance boreholes made in 2010 located the thickest channel fill sequence. From this location, 8.5 m of laminated deposits was retrieved, reaching down to the sandy channel base. Core segments were stored in sealed PVC-tubes in a refrigerator to prevent oxidation and fungus growth. After opening, cores were photographed and sedimentary characteristics described down to the level of individual laminations, and samples were taken for sedimentary analysis and various dating techniques. The investigated flood deposits have formed fairly recently and are located below the present water level, so limited compaction has occurred. Friction and pressure exerted by the piston corer compressed sediments slightly. Coring depths were carefully recorded and were used to stretch the recovered material to original depths. The bottom of each core segment equals its true depth, so stretching was applied linearly (no intra-core changes in bulk densities were detected), and extending to the bottom of the core segment above.

3.1. Grain-size measurements

Continuous samples for grain-size analysis were taken with a semi-regular sample thickness of 1–2 cm. Sample intervals were slightly adjusted to correspond with visual flood layering. Laminations thinner than 1 cm were not sampled individually, due to the minimum required sample volume. Because some flood event-layers were thicker than 2 cm, adjacent samples may reflect stages within a single event. In those cases, which likely also represent the largest floods, the coarsest sample was adopted for comparison with measured peak discharges. Samples were successively pre-treated with 10 ml 30% H_20_2 to remove organic matter, with 5 ml 10% HCl to remove calcium carbonates, and with 300 mg of $Na_4P_2O_7.10H_2O$ to further disperse grains (Konert and Vandenberghe, 1997). Grain-size distributions ranging from 0.1 to 2000 μm were measured in 56 classes with a Sympatec HELOS KR laser-diffraction particle sizer available at the VU University, Amsterdam.

3.2. Descriptive statistics and End Member Modelling

The median, mean, MS, P95, and the EMM-derived proportional contributions of coarser end-members describing the grain-size distributions were calculated. The median and mean are based on the entire grain-size distribution, whereas MS, P95 and EM describe the coarse tail of the grain-size distribution. For EMM, the DRS-Unmixer model (Heslop et al., 2007) was used to unmix different populations. For each site, a model with five EMs was established to characterise the measured sample grain-size distributions (Fig. 2). The use of EMM on fluvial deposits is explorative, as it allows decomposition (or unmixing) of grain-size distribution datasets into a series of distinct grain-size populations, to which a physical meaning is assigned on sedimentological (following interpretations of CM-diagrams by Passega, 1977) and hydrodynamic (e.g., Benedetti, 2003) grounds. Mixing models with more EMs explain a larger proportion of measured distributions, but adding more than five EMs did not lead to significant improvement and was not considered geologically meaningful (following practices established in Weltje, 1997; Prins et al., 2000).

Because the distance between the two research locations is less than ~40 km and sediment is distributed from the same source during flooding events, EMs obtained for ZG and BAR are similar (Fig. 2). Small differences in the grain-size characteristics of EMs (especially the coarsest, EM1) is explained by site-specific factors, such as the distance and connectivity of a sediment trap to the active river (Prins et al., 2000; Erkens et al., 2012). For characterising flood magnitudes with EMM, only the two coarsest end members (EM1 and EM2) were used. Finer EMs represent suspended and wash load populations, for which it is assumed that limited differentiation occurs between different flood magnitudes (Fig. 2), as these fine particles are also in suspension during normal flow and minor floods. This assumption is supported by nearly identical wash load end members at the different research locations, and the apparent admixture of different grain-size populations in deposits belonging to floods of different magnitudes (Fig. 2). Another reason to exclude wash loads in further analysis is that wash load volume and coarseness correlate poorly with peak discharges, because they are heavily influenced by flood wave hysteresis-effects during rising and falling flood stages (Asselman, 1999; Benedetti, 2003). For bimodal grain-size distributions, as characteristic for flood beds (Fig. 2), EMM is an adequate tool to assess data, as mixed populations and the distribution of these EM are site-specific, and are statistically established from the full array of grain-size distributions present in the entire sequence.

Changes in the distance and connectivity of the sediment trap to the active channel (gradually or abruptly) and infilling processes related to water depth (e.g., encroachment of vegetation and turbulence in shallow water) commonly cause distinct phasing in the accumulation of sedimentary fills (e.g., Toonen et al., 2012; Minderhoud et al., 2013). To prepare records for flood magnitude analysis, normalisation of data is required to allow uniform treatment of samples coming from different phases of sedimentation in the record. Without normalisation a phase with a relatively-nearby position of the active river would be mistaken for a period with larger floods, because in the representative section of the record a reduced travel distance signals as delivery of generally coarser material. The identification of section breaks followed from change point analysis (CPA; Taylor, 2000) carried out on grain-size descriptors. Trend-breaks exceeding a 95% confidence level were used to separate different sections. Data in the separated sections were linearly detrended, and grain-size data was normalised into Z-scores per section. Using Z-scores (standard scores) allows to unify the data across different sections. In later steps, flood magnitudes are calculated as a function of the Z-scores. Effectively, these calculations use event-bed coarseness expressed relative to the background value in the respective section of the floodplain lake fill. This background sedimentation represents the fines deposited during minor floods and waning stages of major floods that form the bulk of lake fills and has a composition dominated by EM3–5 (Fig. 2).

3.3. Age-Depth modelling

Meaningful comparison of sedimentary data from individual flood beds with time series of discharge data and historical flood events demands highly accurate age-depth models. Several dating techniques were combined to provide tie-points for the initial age-depth model; (i) XRF and traditionally acquired pollutant-geochemistry were used to pinpoint the onset of heavy-metal pollution contemporaneous with the Industrial Revolution (~AD 1860 in the Lower Rhine), and a short-lived sharp decrease in pollutants during World War II (Middelkoop, 1997), (ii) palynological information marks the presence or absence of specific time-indicator species (e.g., maize, pine, buckwheat, an rye), (iii) ^{210}Pb-dating provides absolute ages in the last century, and (iv) historical documents provide information about the year of channel disconnection or dike breach, which correspond with the base of the sequence, and major adjustments to the floodplain and river, which are reflected as changes in sedimentary style, accumulation rates, and facies. These various constraints were used to create initial stepped-linear age-depth models.

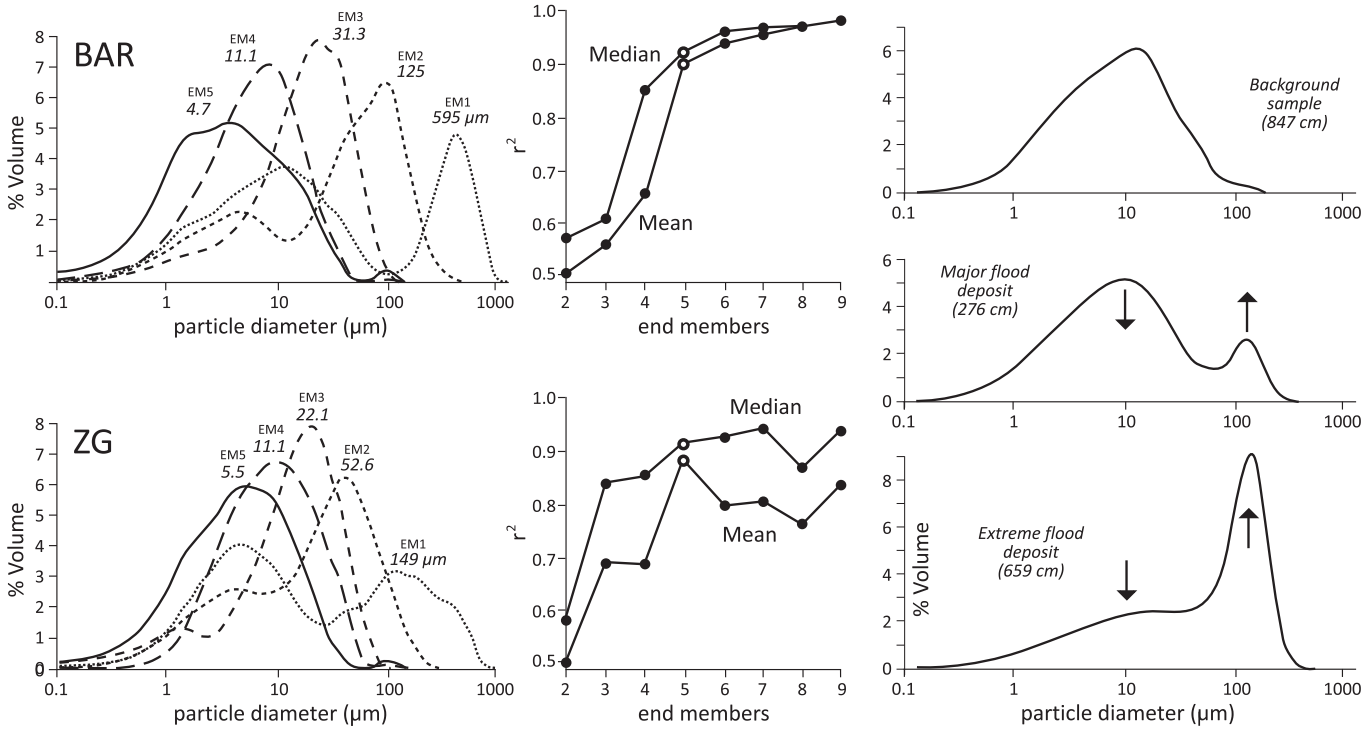

Fig. 2. Grain-size distributions in a 5-end member model, and coefficients of determination (mean and median R^2-values of the fit of EMMs on all grain-size bins) for models using a different number of end members. The right panel depicts 'typical' grain-size distributions of the BAR (depth of plotted samples indicated in cm) associated with deposits from various flood magnitudes — showing the successive admixture of a coarse grained population with increasing discharge.

The initial age-depth model was then further optimized by using the event chronology of historical floods. Known large floods of the last five centuries (Buisman, 2000, 2006; Herget and Meurs, 2010; Toonen, 2013a) should correspond with the coarsest flood beds in the cores. Conservatively following this assumption, extra tie-points were specified in the age-depth model. First, the four largest events were selected from historical records, identified by numerous dike breaches and a regional impact of flooding (AD 1595, 1658, 1809, and 1861; Buisman, 2000, 2006; Toonen, 2013a). Starting with the coarsest imprint in the sedimentary record, spikes were correlated with historical events, using the initial age-depth model as a reference for approximate age — correlations were only considered plausible if historical records corresponded with suggested age-depth modelled ages (generally within a decade). Initial age-depth modelled ages were updated with each added tie-point, based on plausible correlations, after which a next coarsest flood layer was assessed. This process was repeated until all major historical floods and most moderately large events of the last centuries were assigned to a flood layer. Apparent uncorrelated events, not found in either historical records or in the sedimentary record, were further investigated. Possible explanations are discussed later (Section 4.4) in conjunction with a general discussion of the performance and validity of resulting age-depth models.

3.4. Linking flood-bed coarseness to observational discharge series

The age-modelled flood events from after AD 1772 were correlated with the observational discharge series from Lobith (Fig. 1). For each research location, a linear regression was calculated between normalised grain-size descriptors and measured discharges. The coefficient of determination (R^2) was used to quantify performance. The resulting regression functions were applied to the deeper sections of the core (before AD 1772), to reconstruct discharges back to the mid-16th century. Comparing results from temporally overlapping sites allowed to investigate the method accuracy, and the spatial variability in sedimentary flood registration. An independent check on the relation between grain-size distributions of deposited material and discharge comes from Middelkoop and Asselman (1998), who collected overbank sediment deposited during the AD 1993 flood (10,940 $m^3\ s^{-1}$ at Lobith) in the direct vicinity of ZG, using artificial turf sediment traps in a cross-floodplain transect. The then sampled material was reanalysed in this study, subjected to the same procedures and methods as used on all other samples (including EMM and Z-score calculation; considered as a part of the upper section of the ZG scour fill, and normalised accordingly).

4. Results

4.1. Fill sedimentology

The sedimentary fill at both locations shows a phasing of channel filling that in Lower Rhine examples is commonly observed (Toonen et al., 2012). From bottom to top, this comprises (i) a phase of bed load deposition, from the time of cut-off initiation and gradually reducing continuous flow, overlying the coarse-grained basal lag from the last stage of full river flow, (ii) a phase of deposition of relative coarse and thick flood beds at the base of the fill, which gradually decrease in thickness upward into (iii) the main part of the sedimentary sequence consisting of strongly laminated fines of varying coarseness, that is covered by (iv) non-laminated surface-affected deposits from a final phase that marks the transformation of the lake into a terrestrial floodplain environment (Fig. 3).

The base of the sequence in the BAR core features a relative coarse layer (the top ~25 cm was sampled). This layer probably spans a few years to decades only, and is the channel disconnection-related part of the fill. This initial phase of fill accumulation is referred to as 'shallowing' in Toonen et al. (2012). It recorded gradually reducing flow velocities and a gradually decreasing influx and trapping of bed load, which signals that channel entrance plugging and disconnection from the main channel developed rapidly after the initial chute cut-off (Toonen et al., 2012). In the rest of the BAR sequence, deposition into the disconnected

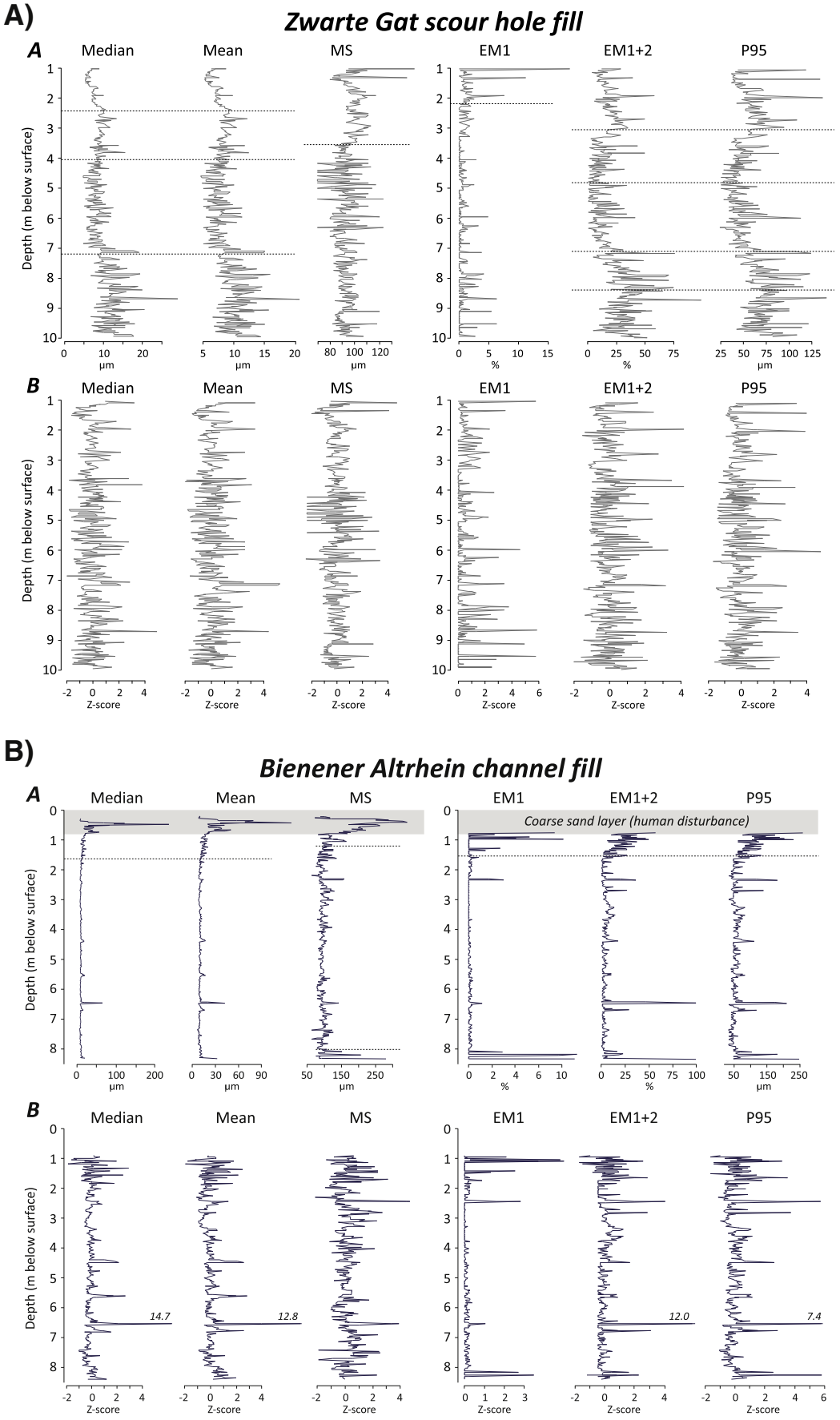

Fig. 3. Raw grain-size data (A) and normalised Z-score data (B). Sections in the sedimentary sequences are illustrated by dashed lines in the raw data at the location of identified change points.

channel occurred during flooding events only, and has resulted in relatively uniform channel fill facies of laminated deposits (Fig. 3); no major breaks in sections are seen, other than at the very top (CPA-confirmed; see below). Distinct layers of relatively coarse deposits, presumably marking large flooding events, are distributed throughout the laminated fill section. The coarsest bed is found at ~6.5 m core depth (Fig. 3). From ~1.5 m depth upwards, the grain-size of the bulk of the laminated deposits starts to increase. Such gradual facies changes at the top of the fill were also observed in previous studies (Toonen et al., 2012; Minderhoud et al., 2013), and mark the transformation from subaqueous to terrestrial conditions (including the encroachment of vegetation). The upper metre of the fill consists of non-laminated coarse sand. The bright yellowish colour, high angularity, large grain-size, and poor sorting of this top layer make it deviate strongly from fluvial deposits encountered in the channel fill below and the nearby floodplain. These sands are regarded to have been introduced in the 1920s, during the construction of a sluice at the point where the BAR channel connected to the Griethorther Altrhein (Fig. 1). Hence, samples from these levels onwards were excluded from End Member Modelling and palaeodischarge prediction.

The laminated sections of the ZG sequence are more variable in their grain-size signals than the BAR sequence (Fig. 3). Scour holes are essentially created during a single flood, and are not gradually disconnected from the active channel, and normally no facies corresponding to a disconnecting-phase exist. The general coarseness and abundance of sandy event layers change importantly around 7 and 4 m core depth. In the lower section (7.0–9.8 m), sandy layers occur frequently and the background matrix is relatively coarse (fine silts rather than clays). Around 7 m, there is a sudden shift towards finer background sediments (Fig. 3). Coarse event-layer interbedding remains frequent, although their average coarseness decreases along with fining of the matrix. This shift can be explained by an altered floodplain configuration, affecting flood-stage connectivity of the scour hole pond with the active river (via the small ditch running adjacent to the scour hole; Fig. 1), and/or by a change in the distance to main channel thalweg due to a southward shift of the main channel and accretion of large gravel bars at the northern bank (Fig. 1). The upper section shows decreasing coarseness and a decreasing occurrence of event layers, although several very coarse flood layers are found near the surface. Besides changes in floodplain connectivity and geometry (e.g., distance to river thalweg, vertical channel bed movement, and ongoing floodplain deposition), this change may also be due to the limited remaining water depth in the scour hole. Especially in this last stage of scour filling, turbulence exerted by flow in the inundated floodplain during major events may have reworked material from the top of the fill. Another explanation can be sought in river engineering measures (e.g., the construction of groynes and removal of sand bars), which has resulted in thalweg lowering (Ten Brinke, 2005), thereby possibly influencing the entrainment of coarse grains at stages of peak discharge and their delivery to the floodplain.

4.2. Raw grain-size data analysis

Although the various grain-size descriptors show similar trends and produce the largest peaks associated with event layers at the same depth, especially the resolution and sensitivity of recording moderately-sized peaks differs importantly (Fig. 3). The median and mean grain-sizes of the entire distribution resolve few coarse-grained event layers. This is mainly due to the poor sensitivity of these descriptors of bulk characteristics to changes in the coarse tail of grain-size distributions (encountered in far fewer flood layers). Especially at site BAR, differentiation in flood layer grain size is poorly resolved using median and mean grain-size descriptors. An increase in observed detail occurs when MS, P95, or EM contributions are used to identify and characterise flood layers. These descriptors all focus on the coarse part of the grain-size distribution. The variance in sedimentary registration demonstrates that especially the transport and deposition of sandy particles is sensitive to floods of variable magnitudes. This implies that during increasing discharge, coarse grains are increasingly admixed to the suspended load (similar to previous observations by Passega, 1964), while fines are present in the suspended load all the time. Such simultaneous entrainment of coarse sands and fines and their simultaneous delivery to the floodplain is also indicated by the bimodal grain-size distributions of EM1 and EM2 (Fig. 2).

The use of solely the very coarsest element in the grain-size distribution to characterise flood deposits can lead to erroneous results, as only very few grain-measurements fall in the considered coarse-grain class. This influences accuracy and reproducibility, especially for MS and EM1. In the MS results (Fig. 3), it can be observed that values for some samples are at the lower limit defining the sand fraction (63 μm). Closer investigation of the full grain-size distribution indicates a complete absence of sand and very coarse silts in these samples. The few hits in the fine sand classes in these measurements often turn out to be caused by flocculates and organic fibres, that survived sample pre-treatment in small quantities. The noise that this adds to MS measurements can influence applications therefore severely. For EM1, the lack of registration of this EM in many samples in between coarser flood beds complicates its use. When normalised, this descriptor gives a Z-scores distribution that differs from other grain-size descriptors (Fig. 4). Especially for moderate Z-scores, this means that the EM1 score refers to a different probability and thus a different magnitude. Additive inclusion of the EM2 descriptor largely resolves this issue, although it also reduces the Z-score of several coarsest event layers. At more proximal locations in the floodplain, the use of EM1 only may be sufficient for registration for floods of all magnitudes. For research locations in intermediate positions in the floodplain and lacking an open connection with the main channel, the added-up use of more coarse-grained EMs increases performance of identifying moderately large events.

4.3. Z-scored grain-size data

In general, Z-scored measurements show details in the record more-sensitively and uniformly than the raw data plots. This is most obvious for median and mean grain-size (Fig. 3), but it also has an effect on the coarse-tail descriptors. From counting event layers, defined as maxima (peaks) in the dataset, with the grain-sizes expressed as a cumulative distribution of Z-scores (Fig. 4), it becomes clear that event registration is similar for all data types, with exception of EM1. It has to be noted, however, that especially results for layers belonging to the allegedly largest/coarsest events are associated with a wide range in Z-scores among different descriptors (Fig. 3). The number of identifiable events matches floodplain inundation recurrence times of the Lower Rhine. Smallest recognised individual flood events in the ZG and BAR records respectively have an average recurrence time of 3.2 and 4.1 years (number of events divided by the time interval), at present roughly corresponding with discharges exceeding 7500 $m^3 s^{-1}$ at Lobith (Fig. 1; Toonen, 2013a). From this it can be concluded that background sedimentation – i.e. core matrix samples not recognised as specific event layers – indeed mainly represents stages of flood sedimentation delivered by minor discharge peaks or deposited during the waning stages of larger floods (post peak discharge).

Z-score normalisation in combination with CPA-analysis has some disadvantages. Z-scores for selected descriptors are calculated using the mean values of that descriptor and its standard deviation, as determined over individual sections. Where these are of limited thickness (short duration) and contain small numbers of samples, the result may be biased. This is considered to be an issue in the uppermost parts of the BAR and ZG sequences, where Z-score normalisation

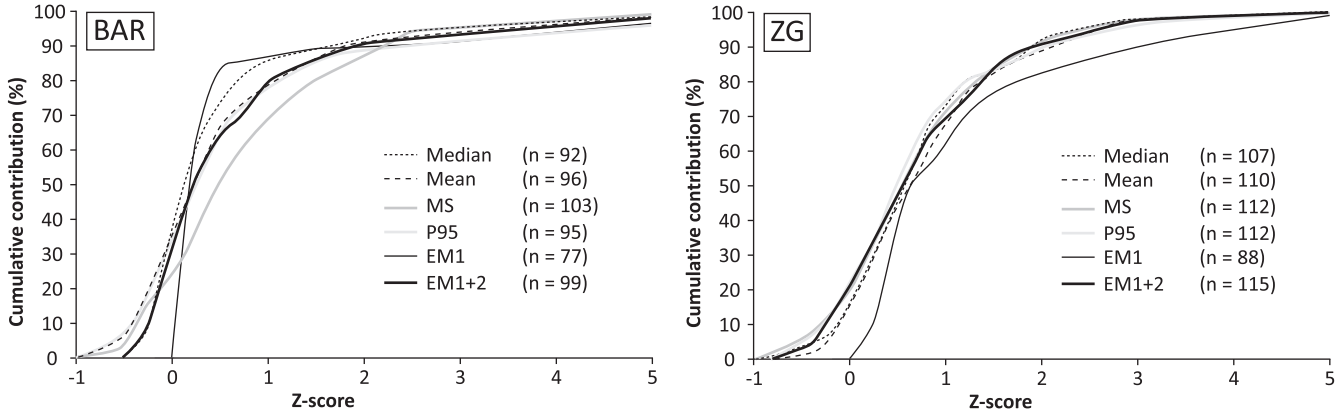

Fig. 4. Cumulative contribution of flood bed Z-scores and number of identified events per grain-size descriptor.

appears unable to completely remove anomalous trends. Still the frequency and scores of event layers differ from lower sections of the cores. It is however also possible that the uppermost parts hold a valid sedimentary representation of changes in fluvial dynamics and the natural distribution of floods.

4.4. Age-Depth models

4.4.1. Bienener Altrhein

Information from various sources (Table 1) provided initial age-depth models for each site (Fig. 5). For the BAR oxbow many age tie-points are available in the upper metre of the sequence; recent deposits at the surface (at the moment of sample collection in 2010), palynological information, sand introduced during the construction of the sluice (AD 1920), and pollution data all suggest deposition of the upper metre in the last century. Further down, tie-points in the initial age-depth model are more scarce, as palynological information and historical records of the abandonment of the channel are not sufficiently precise for defining specific ages. Historical records and maps, however, bracket the bottom of the core: Braun and Thiermann (1981) suggest the initial chute cut-off to have occurred between AD 1550–1600, while sGrooten's historical map of 1573 already shows a fully disconnected upstream part of the BAR, so the onset of fine-grained fluvio-lacustrine filling at 8.49 metre depth must have initiated between 1550 and 1573.

Further establishment of the age-model was done iteratively. First, ages were assigned to the coarsest flood layers, starting with easiest targets (black dots in Fig. 5). These easy targets were: known very large events (e.g., AD 1658, 1784, 1809, 1861), clusters of known large events (e.g., AD 1595–1602, 1651–1658, 1709–1711, 1726–1729, 1882–1883), and relative isolated large floods, occurring in decade-long periods with no other candidate-major floods (e.g., AD 1784, 1882–1883). The iteration result was checked by looking at the interpolated ages for the additional moderately large floods as identified from the sedimentary record (white dots in Fig. 5). These were compared with historical descriptions of local incidental dike breaching in the wider region (Buisman, 2000), with many positive matches identified. The final age-depth model at max deviates several decades from the initial linear model and coarse flood layers line up well with historical information. This implies that historical-sedimentological flood event correlation is useful for establishing age-depth models in such fluvio-lacustrine sequences, when traditional dating techniques cannot be deployed or provide limited accuracy.

With the established age-depth model, three phases of differing sedimentation rates were revealed (Fig. 5; other phases than in Fig. 3). A lower phase (BAR-I) with moderate sedimentation rates, and recording of many moderate-magnitude events, a middle phase (BAR-II) with increased sedimentation rates, also with many moderate-magnitude events which are though rather poorly correlating with historical records, and an upper phase (BAR-III) in which sedimentation rates decreased, but with registration of many large events.

The gradual increase in sedimentation rates at BAR during the 17–18th century (Phase I and II), can be related to migration of the then active channel. The steadily approaching active channel (inset Fig. 1; AD 1550–1819 bend migration) resulted in increasingly efficient sediment delivery and overall thicker flood deposits. Changed proximity of the research location also may explain why sedimentation rates

Table 1
Dating information used as tie-points for the initial age-depth models.

Site	Depth (m)	Age AD	Type	Source
BAR	0.00	2010	Current waterfront	Personal observation
	0.30	1900–1975	Channel fill	Palynology; *no hemp/maize, much rye/pine*
	0.81	1920–1930	Sand layer	Construction Dornicker sluice
	1.10	1860–1870	Channel fill	Onset heavy metal pollution (XRF-scans; unpublished)
	1.84	Before 1880	Channel fill	Palynology; *much hemp and buckwheat*
	8.49	Before 1573	Bed load deposits	Historical map (sGrooten, 1573)
	>8.49	After 1550	Channel base	Historical records (Braun and Thiermann, 1981)
ZG	1.00	Before 1995	Top deposits	Personal observation
	1.21	1991	Top previous core	Middelkoop (1997)
	1.55	1965	Scour hole fill	^{210}Pb-dating (Middelkoop, 1997)
	1.59	1939–1945	Scour hole fill	Temporary dip in heavy metal pollution (Middelkoop, 1997)
	1.89	1940	Scour hole fill	^{210}Pb-dating (Middelkoop, 1997)
	2.24	1915	Scour hole fill	^{210}Pb-dating (Middelkoop, 1997)
	2.70	1860–1870	Scour hole fill	Onset heavy metal pollution (Middelkoop, 1997)
	7.00	Before 1722	Sediment phasing	Historical maps (van Geelkercken, 1639; Couwater, 1722)
	~10.00	1644	Base scour hole	Historical records (Buisman, 2000)

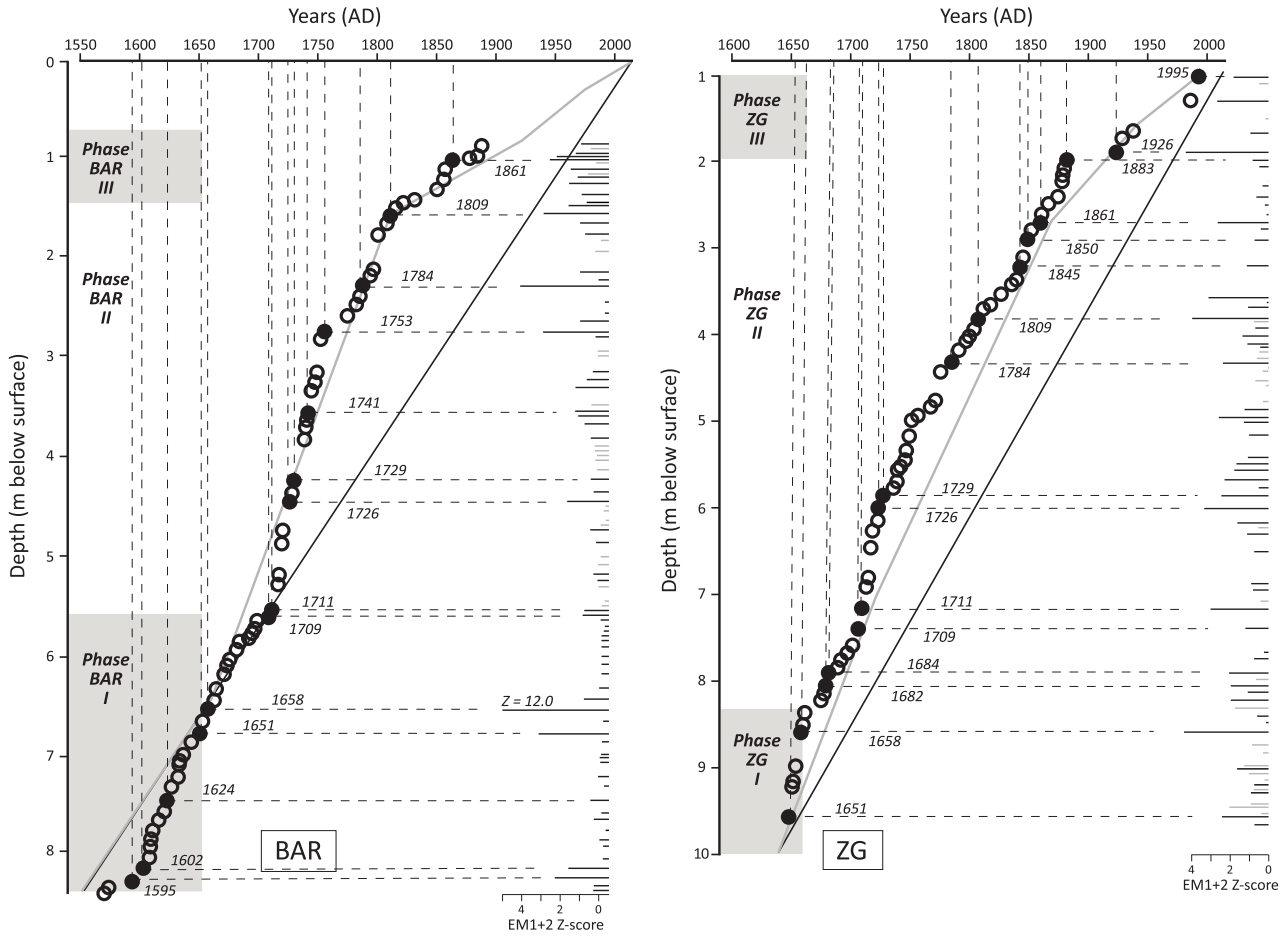

Fig. 5. Initial and final age-depth models. In dark grey, a linear (bottom to top) age-depth model is shown. The light grey line indicates the stepped-linear model (Table 1). The final event-chronological age-depth model is indicated with black and white dots. Black dots are tie-points for the updated model (major events), white dots represent moderate events that are successfully correlated between the sedimentary and historical records. Grey background shades indicate various phases in flood registration and general sedimentation rates. Bars along the vertical axis illustrate flood magnitudes (Z-scores of EM1 + 2); grey bars indicate flood layers that are not correlative with historical records.

suddenly decrease at ~1.5 m, as an artificial channel cut-off in AD 1819 displaced the active channel farther away (Fig. 1). The upper metre with decreased sedimentation rates, yields a comparatively high number of relatively coarse beds. The occurrence of coarse beds in this interval can be attributed to the more frequent occurrence of large floods in the 19th century, while the contribution of sediment delivery during minor floods seems to have decreased. Progressive plug-bar and levee formation at the entrance of the BAR oxbow, and the functioning of the AD 1819 palaeochannel as an additional sediment trap in between BAR and the active channel, presumably reduced background sedimentation at this time.

The relatively high number of flood beds during phase BAR-II that could not be correlated to known floods (Fig. 5) is likely due to migration of the active river, which from AD 1711 onwards induced reworking of the sandy plug-bar that formed following the initial cut-off of BAR. Along the path between the active river and BAR this provided a very local source of extra sand and lowered the discharge threshold for this sediment to be delivered to adjacent lake. Local uptake of sand from this plug-bar, and possibly crevassing into the palaeochannel depression, may explain the 'extra' event beds. In the decades before the AD 1819 diversion, the channel fill temporarily also registered events that did not necessarily exceed bankfull levels, and that are not documented in historical sources either. To avoid over-interpretation of such flood layers in flood magnitude reconstructions, non-correlated events of minor magnitude were excluded from our discharge estimates (Section 4.6).

Vice-versa, there are also several 19th century floods documented in discharge series and historical records, that are not represented by clear event beds in the BAR sedimentary record. Without exception this concerns relatively minor events with peak flows less than 9000 $m^3\ s^{-1}$ that presumably did not result in deposition of sediment coarser than background material or produced thin flood layers that were not resolved in the 2-cm sampling resolution. Moreover, due to a limited thickness they are more easily disturbed than thick layers belonging to major events. Last, fine-grained layers may have been misinterpreted as having formed during the waning stage of larger events (fining top of graded flood layers) when positioned directly above coarse flood beds. Three short periods exist during which many minor historical floods were not reflected in the sedimentary results: AD 1650–1660, AD 1750–1760, and the mid-19th century (Fig. 5). Poor flood registration of smaller events in the 19th century corresponds with the more distal location of the site relative to the river, when the matured plug-bar at the entrance was overtopped during relatively large discharges only. The AD 1750-1760 period is marked in the sedimentary record by thick fine-grained deposits, suggesting that there was active flood deposition, but that the magnitude of these events was too small to be able to distinguish them from the background signal using current methods. For the AD 1650–1660 period, the poor registration has presumably been caused by several major events in the same decade, which obscure or have eroded smaller event layers.

4.4.2. Zwarte Gat

The ZG age-depth model shows a similar discharge registration and phasing of infilling as recorded at site BAR, with gradually decreasing sedimentation rates to the surface (Fig. 3). Again, most dating information is available in the last century, which makes this part of the initial age-depth model best resolved. The exact year of scour hole-formation is documented (AD 1644; Buisman, 2000), which strengthens the quality of the initial age-model considerably.

Ages assigned to coarse event layers mark the same events as in the BAR. Site ZG has filled more gradually until recent times. This allows for a higher record resolution and recognition of more large events and inclusion for tie-points for the age-depth model in the late 19th and 20th century (e.g., 1883, 1926, 1995; Fig. 5). The iterated age-depth model resembles sedimentation rates of the initial model, albeit that the age-depth relations have shifted to older ages. Also, the age model in the lower part of the sequence is somewhat altered, with higher sedimentation rates in the lower part (phase ZG-I), and gradually decreasing sedimentation rates further upward (phase ZG-II). The transition between the two lower phases is dated to the late 17th century, shortly after formation of the scour hole. Three plausible explanations for the gradually lowering sedimentation rates at ZG can be found in the local geomorphology (Fig. 1). Reconstruction of the location of the main river, based on series of historical maps (van Geelkercken, 1639; Couwater, 1722; von Wiebeking, 1800; Beijerink, 1809; Goudriaan, 1830; Bonneblad 532, 1890), indicates a rapid southward migration of the main channel and the formation of extensive gravel bars on the northern bank of the river soon after the ZG was formed. Latest by AD 1722 (Couwater, 1722), the thalweg of the active river became located near the southern main dike, which may have decreased sedimentation rates in the northern part of the floodplain and ZG. An alternative explanation can be sought in the connectivity of the ZG with the main river by a small ditch (Fig. 1). On some historical maps (e.g., Beijerink, 1809), an open connection exists between this ditch and the scour hole. Closure of this open connection and gradual infilling of the ditch probably influenced the transport of sediment between the active river and ZG, and this may have induced the (gradual) decrease in sedimentation rates. A third reason for decreasing sedimentation rates may be the construction of the upstream Pannerdens Canal in AD 1707, which redirected more discharge to the northern Nederrijn distributary (Fig. 1), leading to reduced discharge and sediment transport in the Waal channel at ZG (van de Ven, 1976).

The upper phase (ZG-III) is relatively fine-grained, but this is unlikely to simply resemble reduced proximity to the active channel, as engineering works forced the river thalweg to a location closer to ZG, at the end of the 19th century (inset Fig. 1; formation of southern bank). In recent times, bed degradation has accelerated in response to the fixation and narrowing of rivers by groynes, and ongoing floodplain deposition further increased the difference in elevation between river water levels and the floodplain with the scour hole. Despite increased proximity, this could have raised the threshold discharge at which admixed coarser-fractions can be delivered to the floodplain. However, significant lowering of river bed levels started in the mid-20th century only (Ten Brinke, 2005; Toonen, 2013a). Imprints of moderately-sized floods are lacking in Phase ZG-III, while they are present in the discharge series (Toonen, 2013a). The top interval of the fill thus contains an incomplete flood record. Probably due to an increased elevation difference between channel and floodplain, only largest events have registered with the relative thick fine-grained deposits formed as (re)settling material during the waning stages of these large floods.

4.5. Relating normalised grain-size data to discharge series

The grain-size data for the two sites have a different overlap with the observational discharge series. Site BAR allows a comparison of different data types from AD 1772–1920. Site ZG allows comparison from AD 1772 to present, although recent decades have been recorded fragmentally in the sedimentary record. The AD 1784 flood was excluded from establishing the BAR regression; this year is marked by a severe winter (IJnsen, 1981), with major ice-jamming in the Lower Rhine (Driessen, 1994), which locally raised water levels and caused many violent dike breaches. At BAR, this probably disturbed discharge-sedimentation dynamics, because the Z-score for this event is considerably higher than for any other flood in the last centuries (Fig. 6), while the discharge was not that extreme (Toonen, 2013a).

The regression analysis between grain-size data and discharges (Table 2) demonstrates that median, mean, and MS are fairly poor predictors of flood magnitudes — as earlier studies of bulk properties of suspended load also concluded (e.g., Benedetti, 2003). In contrast, P95 and EM1 + 2 show a clear linear relation between flood peak discharges and the coarseness of deposited material. The use of only EM1 results in a very poor correlation, due to the limited identification of moderately-sized events. Addition of EM2 to EM1 greatly increases performance. In other words, using just the low proportional abundance of the coarsest end member (EM1) for estimating flood magnitudes is error prone, while instead, the slightly more conservative descriptors (P95 and EM1 + 2) are more robust options. These summarise a larger part of the grain size distribution data set and discriminate a larger range of flood magnitudes.

Deposits collected in a transect across the inundated floodplain at ZG at the time of the AD 1993 flood (Middelkoop, 1997), provide an independent check on the established regression between sedimentary and discharge data. EM1 + 2 Z-scores of surface sample grain-sizes from the distal parts of the floodplain reach values up to 0.72. However, Z-scores are on average only 0.39 for this event, and sediment coarseness shows more correspondence with the local floodplain topography than with peak discharges. Z-scores of these surface samples correspond poorly with the trend line of scour fill samples and measured discharge (10,940 $m^3 s^{-1}$ at Lobith), as deposition of coarser material is expected during such a major flood. As no ice jamming has occurred in recent decades and because similar sized floods (e.g., AD 1861, 1926, and 1988) fit well to the established regression between EM1 + 2 Z-scores and peak discharge (most variance occurs with moderate floods), other factors must be responsible for this misfit (further discussed in Section 5.1).

4.6. Historical flood magnitudes

For flood beds in the lower parts of the fills (older than AD 1772), the discharge was predicted by applying the EM1 + 2 regression relations for the BAR and ZG site respectively (Fig. 6). For the upper part of the fill (post 1772), which fed the regression analysis, the discharge predictions are also given, to illustrate the performance of the relation (Fig. 7). Only the EM1 + 2 regression relations were used, because regressions with other descriptors yielded lower coefficients of determination, despite the similarities in the distributions of Z-scores (Fig. 4). Within the calibration period (1772–1900; Fig. 7), the only poor prediction is that for the aforementioned year AD 1784 (Fig. 7). The overestimation of this flood at BAR and ZG indicates the regional extent of ice jamming that particular winter, which is consistent with historical records (Driessen, 1994; Toonen, 2013a). Discharge estimates from both research locations correspond well for the 19th century, but start to deviate progressively from the late 18th century to earlier periods (Fig. 7), as ZG systematically produces higher discharge estimates. Comparison with measured discharge in the late 18th to early 19th century suggests the BAR results to correlate more realistically with discharges, although relative few events for verification exist. Although ZG and BAR produce discharge estimates in similar years before AD 1772, systematic higher estimates by ZG continue, which can be a propagation of a calibration misfit in the used regression (Section 5.2).

Based on the BAR sedimentary flood history, two distinct periods in flooding are identified: (i) the 18th century is marked by many large floods, lacking truly extreme events though and including a period of

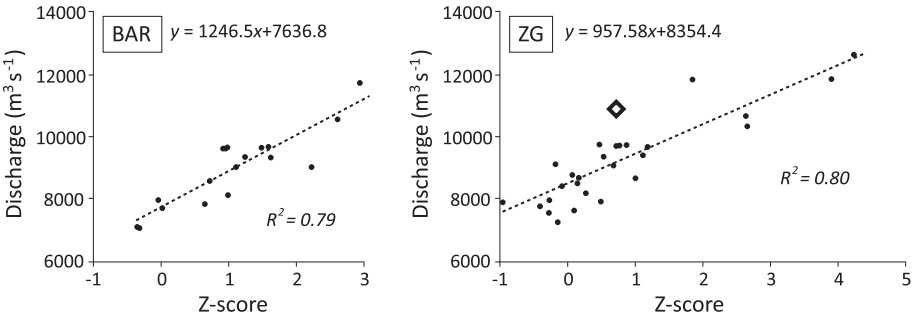

Fig. 6. Regression plots of Z-scored EM1 + 2 data and observed discharges for the same events. The diamond in the ZG-diagram plots the coarsest floodplain deposits of the AD 1993 flood (10,940 $m^3 s^{-1}$ at Lobith; Middelkoop, 1997), sampled in the direct vicinity of the ZG scour hole.

very limited flooding spanning AD 1750–1780, and (ii) the part of the record before AD 1700 with many minor (<8000 $m^3 s^{-1}$) floods, several very large floods (AD 1595, 1651, 1658), and a period of a limited number of flood events from AD 1570–1620. The periods of limited flooding correspond with slightly reduced flooding intensities, inferred from analysis of historical documentary records (Toonen, 2013a).

Largest events, AD 1595, 1651, and 1658, are estimated to have exceeded 10,000 $m^3 s^{-1}$. The BAR estimate for the AD 1658 flood even exceeds 22,000 $m^3 s^{-1}$ (based on an EM1 + 2 Z-score of 12.0). That value seems out of range of meteorological bounds and hydraulic limitations (embankment heights and valley morphology), which limit discharges at Lobith respectively to ~18.700 $m^3 s^{-1}$ and ~15,500 $m^3 s^{-1}$ (Lammersen, 2004). As AD 1658 is marked by a severe winter, and frequent ice jamming of rivers is reported (Buisman, 2000), BAR flood deposition in this year is anomalously coarse, similar to the coarse imprint of the AD 1784 ice-jam flood (Fig. 6). As a test, the EM1 + 2 Z-score was replaced by the lower P95 Z-score of 7.4 (Fig. 3; P95 has a nearly identical Z-score distribution; Fig. 4). This results in a still very high but physically more realistic discharge estimate for the AD 1658 event of ~16.800 $m^3 s^{-1}$. The ZG EM1 + 2 estimate for this flood is much lower, albeit still representing a major event, suggesting a discharge of ~12.600 $m^3 s^{-1}$. This equals the magnitude of the AD 1926 flood, which is the largest discharge recorded in modern observational data series.

Other years may also have been influenced by ice jams, although no extreme discharges are reflected in the sedimentary records. AD 1595 is also associated with a severe winter (Fig. 7), but the regional extent of damage reports in historical records indicates that also large discharges must have been present, which renders the estimated discharge of ~10.500 $m^3 s^{-1}$ plausible. For AD 1651, when certainly no ice jamming occurred, the reconstructed peak discharge amounts 11.500 $m^3 s^{-1}$. An independent estimate for this flood from Cologne (Herget and Euler, 2010), based on historical flood stage indicators, suggests a discharge of at least ~12.000 $m^3 s^{-1}$. Considering the uncertainties in reconstructed discharges (in both studies), our conservative estimate at BAR and effects of flood wave propagation from Cologne to Lobith, we regard the two estimates for the AD 1651 flood to be corresponding.

Table 2
Coefficients of determination for the linear regression between various grain-size descriptors and measured discharges.

Parameter	ZG R^2	BAR R^2
Median	0.49	0.50
Mean	0.51	0.61
MS	0.28	0.60
EM1	0.23	0.15
EM1 + 2	0.80	0.79
P95	0.75	0.72

5. Discussion

The results of this study indicate that Lower Rhine (palaeo-)discharges can be quantified from sedimentary flood records, permitted that data is collected at high resolution and that a descriptor of the coarse tail of the grain-size distribution is used to identify the flood bed, and that normalisation treatments are performed. Even then ~20% unexplained variance remains in the linear regression on carefully age-modelled and statistically processed grain-data (Fig. 6). This indicates that straightforward quantification of grain-size to flood magnitude through linear regression is hindered by several factors, each causing variation in the way floods are registered at and among research locations. These factors include dynamics in local geomorphology, formation of river ice, river management, uncertainties in age-depth modelling, and uncertainties in the correlation between grain-size data and discharges. All these factors propagate into the discharge reconstructions from BAR and ZG (and caused differences among the results obtained for the two sites).

5.1. Geomorphological overprinting

The BAR and ZG case studies show trends in sediment composition and accumulation rates in response to local changes in floodplain geomorphology. Linear detrending and converting proxy data into Z-scores largely eliminates the variation induced by geomorphological change, and results in a more uniform record (Fig. 3). Nevertheless, over intervals with a limited number of samples, gradual changes in Z-scores can still be recognized – i.e. the upper metres of BAR shows many more large floods, which can be caused by natural variability of the flooding regime, but can also relate to insufficiently normalised trends. Over the youngest 450 years, it is possible to compare flood dynamics with discharge series and historical documentation. This gives insight in the most likely explanations for the observed gradual changes in grain-size trends (raw and Z-score standardised), and can help to improve the regression plots and discharge estimates by identification of outliers that are attributed to other processes than peak discharge (Fig. 6).

Especially changes in the connectivity with the main channel, evident at sites ZG and BAR, affects pacing and phasing of channel in-fill and alters recording of coarse flood beds in the fill. To what extent this affects the application of discharge estimation at a site is difficult to assess from an individual flood record only. The two contemporaneous sites, at short distance from each other and along the same main river channel, produced similar flood chronologies, but also show considerable variability. Therefore, building flood chronologies out of sedimentary records of abandoned channels and scour holes becomes more reliable when multiple sites are investigated and compared. Although this can be time consuming, trade-off decisions on the level of geomorphological overprinting in an individual sedimentary flood record can be made more confident once overlap exists with modern discharge records, historical information, and sedimentary records from neighbouring sites. Records of palaeo-environmental change, such as probability density functions of

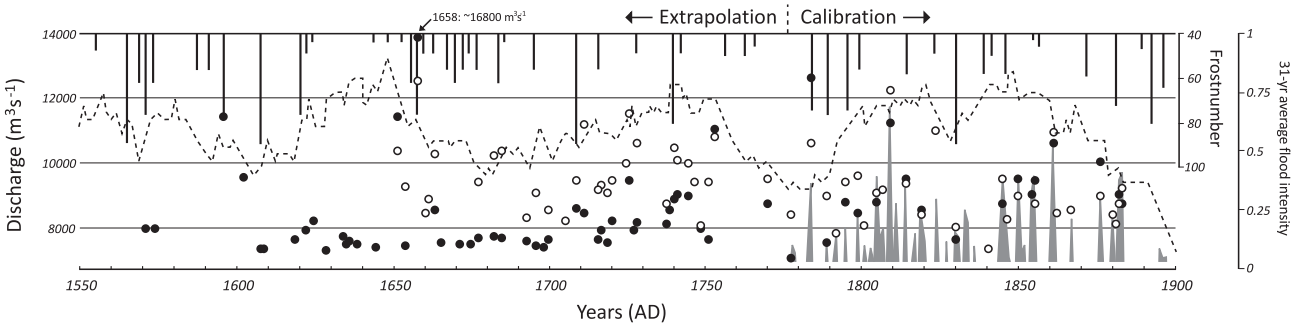

Fig. 7. Discharge reconstructions based on the EM1 + 2-discharge regression for the period after AD 1772. Dark dots represent BAR event layers, white dots ZG event layers, grey peaks (AD 1772−1900) indicate reconstructed discharge for Lobith (Toonen, 2013a). The dashed line indicates an indexed 31-year flooding intensity (Toonen, 2013a), and bars at the top indicate winter severity (number of days of frost; frost number; IJnsen, 1981).

widespread geomorphological changes in fluvial settings (e.g., Hoffmann et al., 2009; Macklin et al., 2012) or avulsion intensity records (Stouthamer and Berendsen, 2001) and other proxy records indicating hydroclimatic variability may be used for comparison. This may confirm the existence of periods of intensified flooding as indicated by sedimentary records in prehistoric times. Such comparisons should also reassess the ways that local overprinting factors were treated in the production of the sedimentary flood history reconstruction.

In this respect, the dealing with the influence of ice jamming can be highlighted as an example. Ice-jamming as a mechanism of inducing large floods when the river carries only moderate discharge has not been frequent all the time. In historical times, ice-jamming occurred mainly during anomalous cold periods, such as the Little Ice Age (Tol and Langen, 2000). Embankment of the Lower Rhine floodplains has worsened their impact, rendering natural flooding into catastrophes, when ice piled-up against high dikes and raised water levels significantly. Both the period of embankment and the Little Ice Age are sufficiently covered by historical records to assess overprinting of the sedimentary record by ice jamming; although insufficient information may be available to correct overestimated discharges, historical records on severe winters and ice jamming may certainly provide caution for calculated discharges in specific years.

A last, so far unmentioned, hydro-geomorphological factor in sedimentary flood registration is induced by the shape of the flood wave. The rate of floodplain inundation and the timing of maximum discharge during a discharge wave determine dynamics that are of importance for the transported material; e.g., flow velocities and hysteresis-effects (Asselman and Middelkoop, 1998; Asselman, 1999; Benedetti, 2003; Berner et al., 2012). In-channel measurements of sediment fluxes and mobile grain-sizes (Frings and Kleinhans, 2008), and analysis of deposited material after the AD 1993 flood (Middelkoop, 1997) indicate a relatively wide range in grain sizes of transported material during a single flood, and among various floods of similar magnitudes. Considerable variability is observed in the coarse event-beds of moderately-sized floods (Fig. 6), which suggests that the coarseness of transported material during these events is influenced more severely by the shape of the discharge wave and hysteresis effects than for floods of higher magnitudes. This also corresponds with independent observations in the Rhine (Asselman, 1999) and Mississippi river (Benedetti, 2003) where quantities and composition of especially fine suspended sediment transport is seen to show strong hysteresis effects and does not correlate well with peak discharge magnitude. Also, spatial variability in grain-sizes and the volume of deposition is likely more influenced by local topography during minor floods with lower inundation levels (Asselman and Middelkoop, 1998).

5.2. Calibration and extrapolation

Both research locations yield good correlations (R^2 = ~0.8; Fig. 6) between coarse-tail grain-size descriptors and measured discharges, which demonstrates the potential of particular statistical descriptors of flood-bed grain size for reconstructing palaeoflood magnitudes. Although current regressions performed well, reconstructions for individual floods at individual sites are prone to considerable uncertainty (Fig. 7). In the period before AD 1772, extrapolated linear-regression discharge estimates are consistently higher for ZG than for BAR (Fig. 7). This persistent offset cannot be explained by natural variability – one would expect uncertainty to be distributed more randomly. Presumably, the difference originates from the limited length of the calibration data at both sites. The calibration period in BAR constrains relatively high Z-scores and great variability (Fig. 3) compared to lower/earlier sections. This may have led the regression to be less sensitive for the variability in registration of moderately-sized floods with low Z-scores. The opposite holds for ZG, where the calibration period is marked by limited variability and registration of moderate flood. From this, one could regard the BAR as minimum discharge estimates, and ZG-discharges as maximum estimates.

Recurrence times associated with reconstructed floods are compared with results of flood frequency analysis (discharge data only; Toonen, 2013a). This provides a rough, but independent check of the quality of generated discharge data. Based on counting peaks that pass certain discharge thresholds, recurrence times for floods of different magnitudes correspond for both sites with recurrence times established from measured discharge data; the range in recurrence times in flood frequency estimates comes from the use of datasets with alternative lengths (Table 3; Toonen, 2013a). From this comparison it is concluded that discharge series from both locations are in line with estimated recurrence times from the last ~240 years. Results from site ZG approach the upper limit (shortest recurrence times) calculated in flood frequency analysis, while at site BAR large events yield slightly longer recurrence times and are placed in the mid-range of flood frequency estimates. BAR recurrence times for moderately large floods (10,000 $m^3\ s^{-1}$) are significantly larger than estimates from ZG and flood frequency analysis. Besides being interpreted as a conservative estimate, the recurrence times derived from the BAR series may also represent truly decreased flooding from AD 1550–1650, as non-stationarity of the flooding regime may cause fluctuations in calculated recurrence times.

5.3. Application to flood research

The results for the Lower Rhine demonstrate the potential of floodplain lake sedimentary records for the construction of continuous flood records and as recorder of local geomorphological dynamics. These records, combined with accurate age-depth models based on existing flood event chronologies, historical information, or other contemporaneous research sites, allow detailed reconstruction of past fluvial environments. Data availability for studying fluvial dynamics and changes in the flooding regime can increase considerably when the approach presented in this paper is applied to other lowland fluvial

Table 3
Peak-over-threshold estimates of the recurrence time associated with flood magnitudes. Counts after AD 1900 come from discharge series; the number of added modern counts, incorporated in the total, is bracketed. Results are compared with flood frequency analysis on discharge series (Toonen, 2013a).

Threshold discharge ($m^3 s^{-1}$)	Count BAR (AD 1571–2012)	Average recurrence	Count ZG (AD 1644–2012)	Average recurrence	Flood frequency analysis (Toonen, 2013a)
10,000	12 (4)	37 yrs	19 (4)	19 yrs	~20 yrs
11,000	9 (3)	49 yrs	9 (3)	41 yrs	40–70 yrs
12,000	3 (1)	147 yrs	3 (1)	123 yrs	90–300 yrs

environments and can be stretched further back in time. Millennial flood records can give important insight in past responses of fluvial systems and flooding regimes to climatic and anthropogenic changes. Knowledge of such relations is not only important for assessing current safety levels with flood frequency analysis, but also for assessment of the impact of future climate change. Moreover, similar detailed natural flood records probably exist in many other low-land regions, also for poorly monitored fluvial systems, which can increase data availability spatially (to a global scale) and allows regional comparison of changing flood dynamics in response to climate and human impact.

6. Conclusions

This study demonstrates that sedimentary archives from abandoned channel fills and dike breach scour holes are suitable as natural flood records. Although changes in the local geomorphology affect sedimentary rates and the coarseness of flood deposits, standardisation and detrending techniques, and comparison with historical records are effective approaches for identification and filtering of local overprints of nearby river activity. This unlocks the sedimentary archive in the fills for flood magnitude reconstruction.

Local overprinting of the main flood record by changes in connectivity, across the floodplains or via tie-channels dissecting plug-bars, is important to filter for, but difficult to assess and to attribute specifically. Because periods of increased connectivity are marked by frequent flood bed formation, historical records and/or multiple channel fill sites with temporal overlap are needed to verify the nature and degree of local overprinting.

When inferring flood magnitudes from grain-size characteristics, using the 95th percentile and/or the coarsest two (out of five) end members is most robust and accurate (Table 2). Bulk grain size descriptors, such as median and mean grain-size, can be used to detect sedimentary trends and within limits provide indication for flood layers, but are not very suitable to provide quantitative estimates of discharges. Although Z-scoring the measurements allows to identify event beds of moderate floods besides those of larger floods (Fig. 3), focusing on the coarsest tail of grain-size distributions yields better information for floods of higher magnitudes.

Age-depth modelling at the studied locations in the last centuries is challenging, as most traditional dating technique do not yield highly precise results (on clayey deposits, largely lacking datable organics) or do not reach beyond the last century (^{210}Pb-dating). It is demonstrated that flood event-chronologies from historical records can be used to improve age-depth relations (Fig. 5). For the Rhine, the timing, cause, and magnitudes of historical floods are very well recorded. As the largest events in the sedimentary records are corresponding well with the historical records, it is possible to assign ages to specific flood layers. These event-based chronologies constrain the range in age-depth models, which in turn makes it possible to assign ages to floods of lesser magnitudes – a progressive approach that allows matching most historical floods to flood deposits with sufficient confidence.

For both research locations it was possible to correlate flood deposits to contemporaneous discharge measurements from the same region. Application of the regression between grain-size and discharge resulted in discharge estimates for historical floods. Year of flooding and relative magnitudes corresponds fairly well among sites and to historical records. However, for the 17th and 18th century, reconstructed discharges from the ZG-scour hole are systematically higher (upper-end estimates) than those for the BAR abandoned channel (conservative estimate) due to calibration issues. This suggests that at these sites detrending and normalisation techniques cannot fully assess local trends in the sedimentary record.

Acknowledgements

The authors thank J. Aloserij, J. Ypma, J. Peeters, H. van Aken (Utrecht University), and F. Smit (now at Aarhus University), for assistance in the field. T. Bäumen (Kreis Kleve) and W. Cornelisse (Waterschap Rivierenland) are acknowledged for giving clearance to respectively the BAR and ZG sites. F. Bunnik carried out palynological analyses (TNO), S. Foulds, S. Rassner, and M. Macklin (Aberystwyth University) are thanked for providing XRF core scan data. M. Hagen, M. Konert, R. van Elsas, W. Wentink, and J. van't Hoff (Vrije Universiteit Amsterdam) are thanked for assistance and guidance in the sedimentary laboratory. This research was funded by Deltares BGS, TNO, and Utrecht University. We thank an anonymous reviewer for useful comments.

References

Arnaud, F., 2005. Discriminating bio-induced and detrital sedimentary processes from particle size distribution of carbonates and non-carbonates in hard water lake sediments. J. Paleolimnol. 34, 519–526.
Asselman, N.E.M., Middelkoop, H., 1998. Temporal variability of contemporary floodplain sedimentation in the Rhine-Meuse delta, The Netherlands. Earth Surf. Process. Landf. 23, 595–609.
Asselman, N.E.M., 1999. Suspended sediment dynamics in a large drainage basin: the River Rhine. Hydrol. Proc. 13, 1437–1450.
Beierle, B.D., Lamoureux, S.F., Cockburn, J.M.H., Spooner, I., 2002. A new method for visualizing particle size distributions. J. Paleolimnol. 27, 279–283.
Beijerink, F., 1809. Kaart van de doorbraak onder Loenen in het Ambt van Overbetuwe voorgevallen op den 10 januari 1809. Rijksarchief van Gelderland, Algemene Kaarten Verzamelingp. 385.
Benedetti, M.M., 2003. Controls on overbank deposition in the Upper Mississippi River. Geomorphology 56, 271–290.
Berner, Z.A., Bleeck-Schmidt, S., Stüben, D., Neumann, T., Fuchs, M., Lehmann, M., 2012. Floodplain deposits: a geochemical archive of flood history — a case study on the river rhine, germany. Appl. Geochem. 27, 543–561.
Bonneblad 532, 1890. Chromotopografische Kaart des Rijks 532. accessed on. www.watwaswaar.nl.
Braun, F.J., Thiermann, A., 1981. Erläuterungen zu Blatt 4103 Emmerich, Geologische Karte von Nordrhein-Westfalen 1:25000. Geologisches Landesamt Nordrhein-Westfalen, Krefeld.
Buisman, J., 2000. Duizend jaar weer, wind en water in de Lage Landen, Deel 4. Van Wijnen, Franeker.
Buisman, J., 2006. Duizend jaar weer, wind en water in de Lage Landen, Deel 5. Van Wijnen, Franeker.
Couwater, J., 1722. Caarte van den Ewijksen en Loenense rijswaarde van de freulens van Wijckraat. Rijksarchief van Gelderland, Algemene Kaarten Verzamelingp. 51.
Chbab, E.H., Buiteveld, H., Diermanse, F., 2006. Estimating exceedance frequencies of extreme river discharges using statistical methods and physically based approach. Osterr. Wasser Abfallwirtsch. 58, 35–43.
Cohen, K.M., Stouthamer, E., Hoek, W.Z., Berendsen, H.J.A., Kempen, H.F.J., 2009. Zand in banen (3e druk). Sand-depth maps of the central and upper Rhine-Meuse delta, including the IJssel valley (with summary in English). Universiteit Utrecht/Provincie Gelderland, Utrecht, The Netherlands (75 pp. + CD-ROM).
Cremer, H., Bunnik, F.P.M., Donders, T.H., Hoek, W.Z., Koolen-Eekhout, M., Koolmees, H.H., Lavooi, E., 2010. River flooding and landscape changes impact ecological conditions of a scour hole lake in the Rhine-Meuse delta, The Netherlands. J. Paleolimnol. 44, 789–801.
Czymzik, M., Brauer, A., Dulski, P., Plessen, B., Naumann, R., von Grafenstein, U., Scheffer, R., 2013. Orbital and solar forcing of shifts in Mid- to Late Holocene flood intensity

from varved sediments of pre-alpine Lake Ammersee (southern Germany). Quat. Sci. Rev. 61, 96–110.
Driessen, A.M.A.J., 1994. Watersnood tussen Maas en Waal. Walburg Pers, Zutphen.
Erkens, G., Prins, M., Toonen, W., 2012. Human impact on the Middle and Late Holocene floodplain sediment characteristics along the River Rhine. EGU Gen. Assem. 2012, 5971.
Frings, R.M., Kleinhans, M.G., 2008. Complex variations in sediment transport at three large river bifurcations during discharge waves in the river Rhine. Sedimentology 55, 1145–1171.
Goudriaan, B.H., 1830. Kaart van de rivieren de Boven Rijn, de Waal, de Merwede en Oude en een gedeelte van de Nieuwe Maas van Lobith tot Brielle. Rijksarchief Gelderland, Algemene Kaarten Verzamelingp. 285.
Herget, J., Euler, T., 2010. Hoch- und Niedrigwasser in historischer und prähistorischer Zeit. Geographische Rundschau 62, 4–10.
Herget, J., Meurs, H., 2010. Reconstructing peak discharges for historic flood levels in the city of Cologne, Germany. Glob. Planet. Chang. 70, 108–116.
Heslop, D., von Dobeneck, T., Höcker, M., 2007. Using non-negative matrix factorization in the unmixing of diffuse reflectance spectra. Mar. Geol. 241, 63–78.
Hesselink, A.W., 2002. History makes a river: morphological changes and human interferences in the river Rhine, the Netherlands. Neth. Geogr. Stud. 292.
Hesselink, A.W., Weerts, H.J.T., Berendsen, H.J.A., 2003. Alluvial architecture of the human-influenced river Rhine, The Netherlands. Sediment. Geol. 161, 229–248.
Hoffmann, T., Erkens, G., Gerlach, R., Klostermann, J., Lang, A., 2009. Trends and controls of Holocene floodplain sedimentation in the Rhine catchment. Catena 77, 96–106.
IJnsen, F., 1981. Onderzoek naar het optreden van winterweer in Nederland. KNMI, Wetenschappelijk Rapport W.R. 74-2.
Knox, J.C., 1993. Large increases in flood magnitude in response to modest changes in climate. Nature 361, 430–432.
Konert, M., Vandenberghe, J., 1997. Comparison of laser grain size analysis with pipette and sieve analysis: a solution for the under-estimation of the clay fraction. Sedimentology 44, 523–535.
Klemeš, V., 2000. Tall tales about tails of hydrological distributions. I. J. Hydrol. Eng. 5, 227–231. http://dx.doi.org/10.1061/(ASCE)1084-0699(2000)5:3(227).
Lammersen, R., 2004. Grensoverschrijdende effecten van extreem hoogwater op de Niederrhein. Eindrapport Duits-Nederlandse Werkgroep Hoogwater.
Macklin, M.G., Fuller, I.C., Jones, A.F., Bebbington, M., 2012. New Zealand and UK Holocene flooding demonstrates interhemispheric climate asynchrony. Geology 40, 775–778.
Middelkoop, H., 1997. Embanked floodplains in the Netherlands: geomorphological evolution over various time scales. Neth. Geogr. Stud. 224.
Middelkoop, H., Asselman, N.E.M., 1998. Spatial variability of floodplain sedimentation at the event scale in the Rhine-Meuse Delta, the Netherlands. Earth Surf. Processes Landforms 23, 561–573.
Minderhoud, P.S.J., Cohen, K.M., Toonen, W.H.J., Erkens, G., Hoek, W.Z., 2013. Oxbow channel fill sedimentology as a tool for age-depth modelling and reconstruction of palaeogeography and fluvial dynamics. In: Toonen, W.H.J. (Ed.), A Holocene flood record of the Lower Rhine. Utrecht Stud. Earth Sci 41.
Nesje, A., Dahl, S.O., Matthews, J.A., Berrisford, M.S., 2001. A 4,500 year record of river floods obtained from a sediment core in Lake Atnsjoen, eastern Norway. J. Paleolimnol. 25, 329–342.
Parris, A.S., Bierman, P.R., Noren, A.J., Prins, M.A., Lini, A., 2010. Holocene paleostorms identified by particle size signatures in lake sediments from the northeastern United States. J. Paleolimnol. 43, 29–49.
Passega, R., 1964. Grain size representation by CM patterns as a geological tool. J. Sediment. Petrol. 34, 830–847.
Passega, R., 1977. Significance of CM diagrams of sediments deposited by suspension. Sedimentology 24, 723–733.
Prins, M.A., Postma, G., Weltje, G.J., 2000. Controls on terrigenous sediment supply to the Arabian Sea during the late quaternary: the Makran continental slope. Mar. Geol. 169, 351–371.
Rijkswaterstaat-AGI, 2005. Actueel Hoogtebestand Nederland (AHN), revised version. Rijkswaterstaat, Adviesdienst Geo-informatie en ICT: Delft.
sGrooten, C., 1573. Comitatus Montensis et trium cornuum Rheni typus 1573 (historical map).
Stouthamer, E., Berendsen, H.J.A., 2001. Avulsion frequency, avulsion duration, and interavulsion period of Holocene channel belts in the Rhine-Meuse Delta, The Netherlands. J. Sediment. Res. 71, 589–598.
Taylor, W., 2000. Change-Point Analyzer 2.0. Taylor Enterprises, Libertyville, Illinois.
Ten Brinke, W., 2005. The Dutch Rhine: a restrained river. Veen Magazines, Diemen.
Te Linde, A.H., Aerts, J.C.J.H., Bakker, A.M.R., Kwadijk, J.C.J., 2010. Simulating low-probability peak discharges for the Rhine basin using resampled climate modeling data. Water Resour. Res. 46, W03512.
Tol, R.S.J., Langen, A., 2000. A concise history of Dutch river floods. Clim. Change 46, 357–369.
Toonen, W.H.J., Kleinhans, M.G., Cohen, K.M., 2012. Sedimentary architecture of abandoned channel fills. Earth Surf. Process. Landf. 37, 459–472.
Toonen, W.H.J., 2013a. Flood frequency analysis and discussion of non-stationarity of the Lower Rhine flooding regime (AD 1350–2011) using multiple-site discharge data, water level measurements, and historical records. In: Toonen, W.H.J. (Ed.), A Holocene flood record of the Lower Rhine. Utrecht Stud. Earth Sci 41.
Toonen, W.H.J., 2013b. A Holocene flood record of the Lower Rhine. Utrecht Stud. Earth Sci. 41.
Toonen, W.H.J., de Molenaar, M.M., Bunnik, F.P.M., Middelkoop, H., 2013. Middle-Holocene palaeoflood extremes of the Lower Rhine. Hydrol. Res. 44, 248–263.
Van de Ven, G., 1976. Aan de wieg van Rijkswaterstaat — wordingsgeschiedenis van het Pannerdens Kanaal. De Walburg Pers, Zutphen.
Van Geelkercken, N., 1639. Kaart van de Waalstroom tegen de heerlijkheid Loenen. Rijksarchief van Gelderland, archief Rekenkamerp. 62.
Von Wiebeking, K.F., 1800. Karte von der Waal, von dem unteren Rhein, dem Leck von der Merwede und der Maas, und von den Gegenden welche an diesen Flüssen liegen. Rijksarchief van Gelderland, Algemene Kaarten Verzamelingp. 281.
Weltje, G.J., 1997. End-member modeling of compositional data: numerical–statistical algorithms for solving the explicit mixing problem. J. Math. Geol. 29, 503–549.
Weltje, G.J., Prins, M.A., 2007. Genetically meaningful decomposition of grain-size distributions. Sediment. Geol. 202, 409–424.